ELSEVIER

Journal of Alloys and Compounds 323–324 (2001) 267–272

Journal of ALLOYS AND COMPOUNDS

www.elsevier.com/locate/jallcom

Site-selective spectroscopy and infrared-to-visible upconversion in a Nd^{3+}-doped $Pb_5Al_3F_{19}$ crystal

J. Fernández[a,b,*], M. Sanz[a], A. Mendioroz[a], R. Balda[a,b], J.P. Chaminade[c], J. Ravez[c], L.M. Lacha[a], M. Voda[a], M.A. Arriandiaga[d]

[a]*Departamento de Física Aplicada I, E.T.S.I.I. y Telecom, Alda Urquijo s/n, 48013 Bilbao, Spain*
[b]*Centro Mixto CSIC-UPV/EHU, E.T.S.I.I. y Telecom, Universidad del País Vasco, Alameda Urquijo s/n, 48013 Bilbao, Spain*
[c]*Institut de Chimie de la Matière Condensée de Bordeaux (I.C.M.C.B.- C.N.R.S.), 87 Av du Dr. Albert Schweitzer, 33608 Pessac cédex, France*
[d]*Departamento de Física Aplicada II, Facultad de Ciencias, Universidad del País Vasco, Apartado 644, Bilbao, Spain*

Abstract

In this work, we analyzed the spectroscopic features of the absorption and emission of Nd^{3+} in a fluoroaluminate $Pb_5Al_3F_{19}$ crystal. Two main crystal field sites were identified for the rare earth in this crystal which may correspond to the two different crystallographic sites of Pb^{2+}. Infrared-to-visible and -ultraviolet upconversion, under continuous wave and pulsed laser excitation, was observed at room and low temperatures. Analysis of the steady-state excitation spectra and of the decays of the upconverted emissions shows that the most likely mechanism for the observed upconversion emissions is an energy-transfer upconversion (ETU) process.

Keywords: Optical properties; Luminescence; Time-resolved optical spectroscopies; Crystal growth; Nonlinear optics

1. Introduction

Recently, there has been renewed interest in solid-state lasers, due to great advances in the development of semiconductor laser diodes, which can be used as pumping sources. Upconversion rare-earth solid-state lasers offer potentially simple and compact sources of visible coherent light.

Among crystalline lasers, those based on fluoride matrices have been studied extensively in the last two decades [1]. The main peculiarities of the luminescence of rare-earth-activated fluoride crystals compared with oxygen-containing compounds are the weak crystal field and weak non-radiative probabilities, resulting in long lifetimes of the excited state and low concentration quenching. These properties can positively affect upconversion pumping schemes, which may allow the creation of visible crystalline lasers with infrared (IR) laser-diode excitation.

In this context, the recently investigated $A_5B_3F_{19}$ compositions could provide a large variety of novel insulating crystalline materials [2] for laser matrices. From these compounds we chose the $Pb_5Al_3F_{19}$ composition because it is possible to grow it as a single crystal with appropriate dimensions. In this report the linear and nonlinear optical properties of Nd^{3+} in a $Pb_5Al_3F_{19}$ single crystal are presented for the first time. This study includes steady-state site-selective emission and excitation spectroscopy, time-resolved measurements, and IR-to-ultraviolet (UV) and -visible (VIS) upconversion under both continuous and pulsed regimes.

2. Structural details

The fluoroaluminate $Pb_5Al_3F_{19}$ (PAF) belongs to the $Pb_5M_3F_{19}$ family with M=Al, Ti, V, Cr, Fe, Ga. Both isolated AlF_6 octahedra and those forming chains along the polar *c*-axis of the tetragonal cell undergo distortions [2]. The sequence of phase transitions is the following:

	← 140 K	← 305 K	← 360 K	←
*I*4 *cm*	→ 270 K *P*4/*n*	→ 320 K *I*2/*c*	→ 360 K *I*4/*m*	→ *I*4/*mcm*
ferroelectric	antiferroelectric	ferroelastic	paraelastic	paraelastic
V	IV	III	II	I

In this work we investigated the optical properties of Nd^{3+} in the ferroelectric phase V. Fig. 1 shows a projection

*Corresponding author. Departamento de Física Aplicada I, E.T.S.I.I. y Telecom, Alda Urquijo s/n, 48013 Bilbao, Spain. Tel.: +34-94-601-4044; fax: +34-94-601-4178.

E-mail address: wupferoj@bi.ehu.es (J. Fernández).

0925-8388/01/$ – see front matter
PII: S0925-8388(01)01029-5

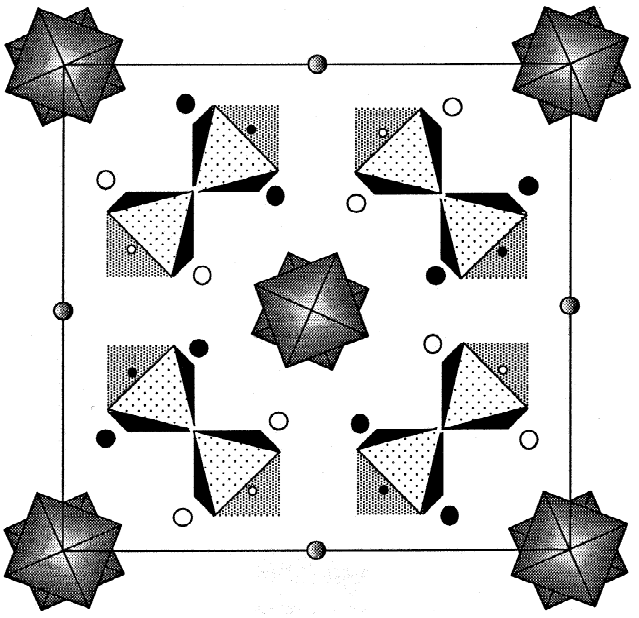

Fig. 1. Projection of the crystalline cell of a $Pb_5Al_3F_{19}$ (PAF) crystal perpendicular to the *c*-axis in the ferroelectric phase V.

of the crystalline cell perpendicular to the *c*-axis. As can be seen, phase V is constituted by chains of AlF_6 octahedra sharing vertices, isolated AlF_6 octahedra, and complex polyhedra constituted by lead and fluorine atoms. In this phase, Pb^{2+} conform to two different kinds of polyhedra, nine- and 10-fold coordinated, respectively [3].

3. Experimental

PbF_2 and NdF_3 were pure Merck and Cerac powders (99.99%). Anhydrous AlF_3 was obtained by thermal decomposition of $(NH_4)_3AlF_6$ under dry argon atmosphere. Crystal growth was performed in a biconical platinum crucible sealed under dry argon. After a preliminary interaction of starting products (15 h at 550°C) the crucible was heated to 720°C in the isothermal zone of the furnace. Cooling was achieved from 720 to 550°C at a rate of 0.5° h^{-1} and from 550 to 20°C at a rate of 10° h^{-1}.

Several monocrystalline pink-colored transparent blocks of about 1 cm^3 were obtained. The crystals were cut in a parallelepiped form and oriented with two of their faces perpendicular to the tetragonal axis. Physicochemical analysis of these crystals gave 1.6×10^{20} neodymium atoms cm^{-3}.

The sample temperature was varied between 4.2 and 300 K in a continuous flow cryostat. Room temperature absorption spectra in the 300–2500 nm spectral range were recorded using a Cary 5 spectrophotometer.

Steady-state site-selective emission and excitation spectra were obtained by exciting the sample with a Ti-sapphire ring laser (0.4 cm^{-1} linewidth) in the near infrared, 780–920 nm range. Fluorescence was analyzed with a 0.22 m Spex monochromator and the signal was detected by an extended infrared photomultiplier and finally amplified by a standard lock-in amplifier technique. The visible fluorescence was detected by a Hamamatsu R928 photomultiplier.

Lifetime measurements were performed by resonantly exciting the $^4F_{3/2}$ multiplet with a Ti-sapphire laser, pumped by a pulsed frequency doubled Nd:YAG laser (9 ns pulse width), and the emission was detected with a Hamamatsu R7102 photomultiplier. The data were processed by an EG&G-PAR boxcar integrator.

4. Results and discussion

4.1. Absorption and emission properties

The absorption and emission spectra of Nd^{3+} in this crystal are characterized by inhomogeneously broadened lines similar to those found in glass materials. The room temperature absorption spectra in the 300–2500 nm spectral range were recorded for both π and σ (electric field parallel and perpendicular to the crystalline *c*-axis, respectively). The spectra are similar for both polarizations. The energy level diagram for Nd^{3+} in PAF obtained from the absorption spectrum is shown in Fig. 2.

As mentioned above, the structural characteristic of the PAF crystal allows the existence of two different sites for

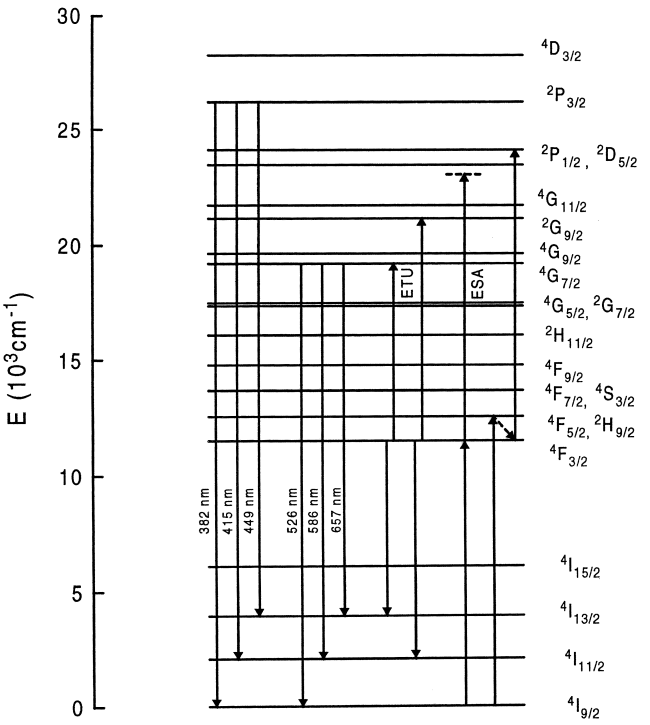

Fig. 2. Energy level diagram for Nd^{3+} in a PAF crystal obtained from the room temperature absorption spectrum. Possible upconversion mechanisms and assignments of the main upconverted emission bands are also indicated.

Pb^{2+}. On the other hand, taking into account the size of the trivalent neodymium ion (104 pm), the most probable place for Nd^{3+} would appear to be a lead site. If this were the case, charge compensation through the introduction of an interstitial fluorine should occur in order to stabilise the PAF structure. As a consequence, some disorder could appear in the coordination number and/or positions of the fluorine ligands constituting the rare-earth polyhedra, giving rise to the observed inhomogeneous broadening; besides, some clustering of neodymium ions could possibly take place. Taking this hypothesis for granted, site-selective investigations were performed in order to identify the different crystal field sites for Nd^{3+} in this crystal. Steady-state and time-resolved site-selective measurements were made by exciting the $^4I_{9/2} \rightarrow {}^4F_{3/2}$ transition.

Site-selective excitation spectra of Nd^{3+} were obtained at 4.2 K. The luminescence was collected at different wavelengths by sweeping the $^4F_{3/2} \rightarrow {}^4I_{11/2}$ emission every 2 Å. For the selected emission wavelengths, instead of the two expected components corresponding to the $^4I_{9/2} \rightarrow {}^4F_{3/2}$ transition, the spectra showed more than one peak for each component. However, as shown in Fig. 3, at two given emission wavelengths, 1046.4 and 1049.1 nm, the low energy component corresponding to the $^4I_{9/2} \rightarrow {}^4F_{3/2}$ doublet spectacularly narrows into almost one single component as should be expected for one well defined crystal field site. As can also be observed, the high energy component of the doublet, which is more tightly coupled to the host vibrations, shows a more complex structure, reflecting the accidental mixing of the emissions coming from the two main crystal field sites that could exist for the rare-earth ion in this crystal. According to the expected random orientation of the optical centres, no differences were observed among the excitation spectra recorded at different polarizations.

In order to confirm if the features shown by the excitation spectra can be unequivocally related to the existence of two main crystal field sites for Nd^{3+} in the PAF crystal, we recorded the site-selective steady-state emission spectra for the $^4F_{3/2} \rightarrow {}^4I_{11/2}$ transition by exciting at 867.6 and 869.3 nm, which correspond to the peak positions of the low energy Stark component of the excitation spectra shown in Fig. 3. Fig. 4 shows the resulting emission spectra obtained at 4.2 K. As can be observed, the features of both spectra clearly show the presence of two different emission centres. Moreover, the number of peaks (which should be six in a low crystal field symmetry) shown by each emission spectrum indicates the presence of some energy mixing due to a still poor wavelength selection and/or to the presence of other residual crystal field sites for neodymium ions.

The lifetimes of the $^4F_{3/2}$ level were obtained at different temperatures and excitation wavelengths along the $^4I_{9/2} \rightarrow {}^4F_{3/2}$ absorption band, and the luminescence was collected at different emission wavelengths in the $^4F_{3/2} \rightarrow {}^4I_{11/2}$ transition. The experimental decays are well described to a good approximation by an exponential function at all temperatures and wavelengths. The lifetimes are nearly independent of temperature in the 77–295 K range.

As expected, if different sites for the rare earth were present, the lifetime values should be dependent on the excitation and emission wavelengths. In our case, due to the noticeable overlapping between the emissions coming from both main Nd^{3+} sites, it is somewhat difficult to give accurate values for the excited state lifetime of each site. Measurements performed at different excitation wavelengths along the $^4I_{9/2} \rightarrow {}^4F_{3/2}$ absorption band show that the lifetime displays a variation of about 15% around 435 μs.

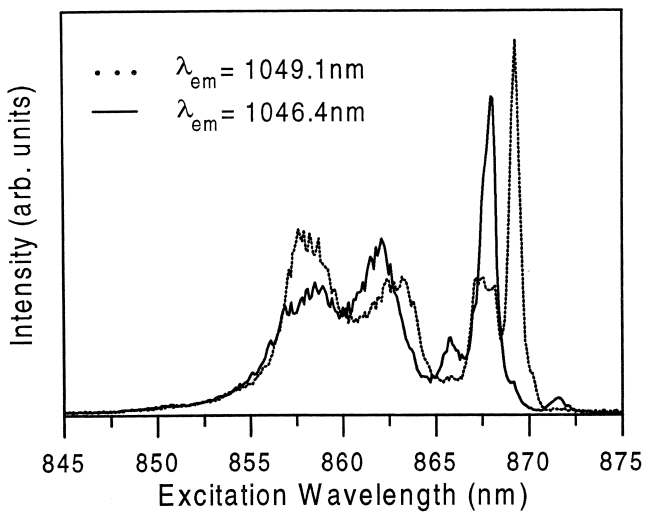

Fig. 3. Steady-state excitation spectra of the $^4I_{9/2} \rightarrow {}^4F_{3/2}$ transition at 4.2 K in a PAF crystal obtained by collecting the luminescence at two different wavelengths into the $^4F_{3/2} \rightarrow {}^4I_{11/2}$ emission band.

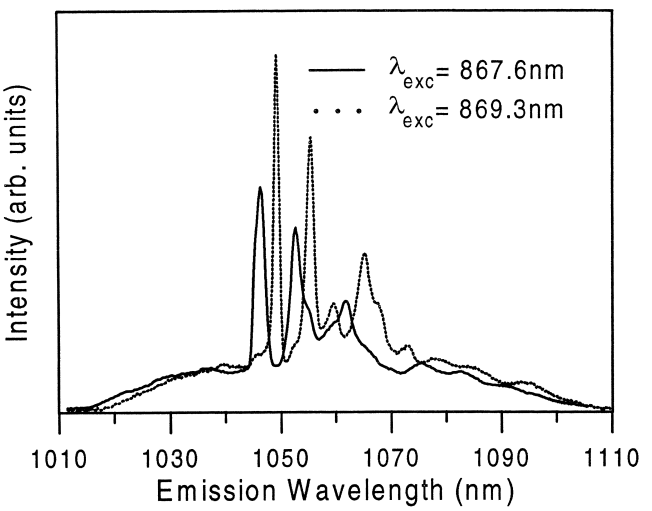

Fig. 4. Steady-state emission spectra for the $^4F_{3/2} \rightarrow {}^4I_{11/2}$ transition in a PAF crystal obtained at 4.2 K by exciting at two different wavelengths into the $^4I_{9/2} \rightarrow {}^4F_{3/2}$ absorption band.

4.2. Infrared-to-visible upconversion

Visible upconversion was observed at room and low temperatures in a Nd^{3+}-doped PAF crystal under continuous wave (cw) and pulsed IR laser excitation. The steady-state emission and excitation spectra were obtained by exciting the samples in the 780–880 nm spectral range using a cw Ti-sapphire ring laser (8 GHz linewidth). Cut-off filters were used to remove both the pumping radiation and the infrared luminescence from the samples. As an example, Fig. 5a shows the upconverted fluorescence in the 350–700 nm region at 77 K by exciting at 796.1 in resonance with the $^4I_{9/2} \rightarrow {}^4F_{5/2}$ transition. The spectra show three main bands located around 526, 586 and 657 nm, two weak blue emissions at 415 and 449 nm, and a UV weak band situated around 382 nm. As can be seen from Fig. 5b, the room temperature upconverted emission bands show a more complex structure due to thermalization processes. Similar spectra were obtained by pumping at 868.1 nm in resonance with the $^4F_{3/2}$ level.

The excitation spectrum of the visible emissions was investigated in the 780–880 nm range (using the Ti-sapphire tunability). Similar excitation spectra were obtained by collecting the luminescence in the green, yellow, and red (526, 586 and 657 nm) regions, in the blue region (415 and 449 nm), or at the UV lines. As an example, Fig. 6 shows the excitation spectrum obtained at 77 K of the upconverted emission at 586 nm. This spectrum shows similar features to that obtained by one photon absorption.

Together with the energy level diagram of Nd^{3+} in PAF, Fig. 2 illustrates the possible mechanisms of population loss from the $^4F_{3/2}$ doublet leading to upconversion processes: excited state absorption (ESA) and/or energy-transfer upconversion (ETU) by pumping either the $^4F_{3/2}$ or $^4F_{5/2}$ manifolds. Concerning the first process, as we can see from Fig. 2, by pumping in the $^4F_{3/2}$ state there is not a good energy matching between the $^4F_{3/2}$ state and $^2P_{1/2}$, $^2D_{5/2}$ multiplets by means of an additional IR photon and therefore we expect a very low probability for such a process. However, if the excitation is made in the $^4F_{5/2}$ level, a second IR photon could allow an upward transition to the $^2D_{5/2}$ multiplet. The second mechanism occurs via a dipole–dipole interaction of two excited Nd^{3+} ions in the $^4F_{3/2}$ state [4,5]. As shown in Fig. 2, in this process one ion is promoted to a higher excited state, whereas the other ion drops to a lower energy state. The magnitude of the upconversion rate is a function of the overlap between the absorption spectrum for the upward transition and the emission spectrum for the downward transition and the

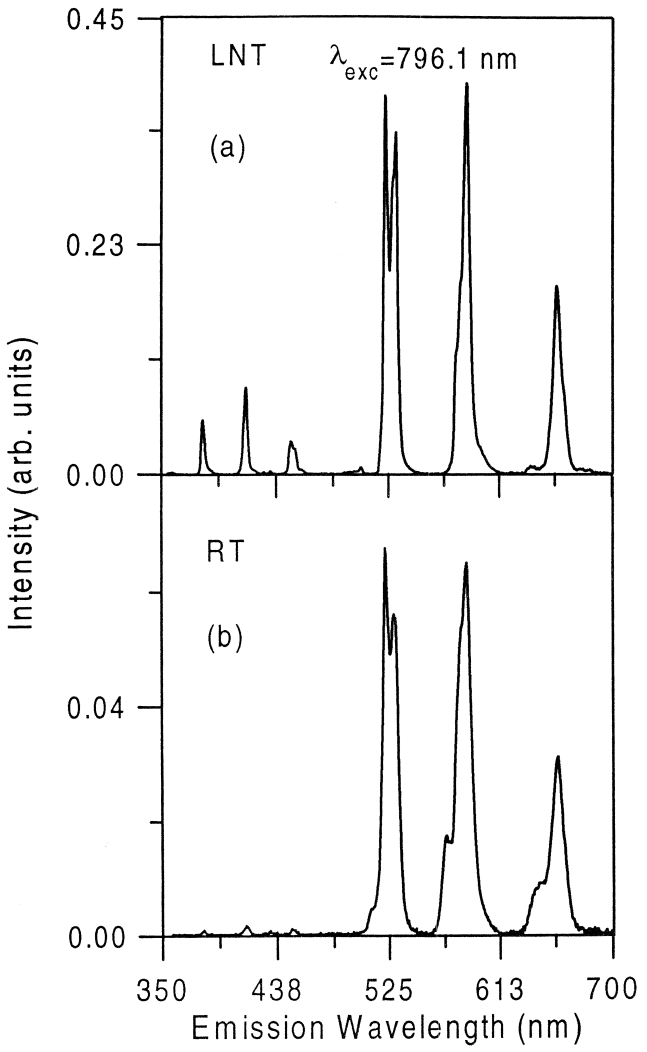

Fig. 5. Upconversion emission spectra in a PAF crystal obtained at liquid nitrogen temperature (LNT) (a), and room temperature (RT) (b) by exciting the sample at 796.1 nm in resonance with the $^4F_{5/2}$ level.

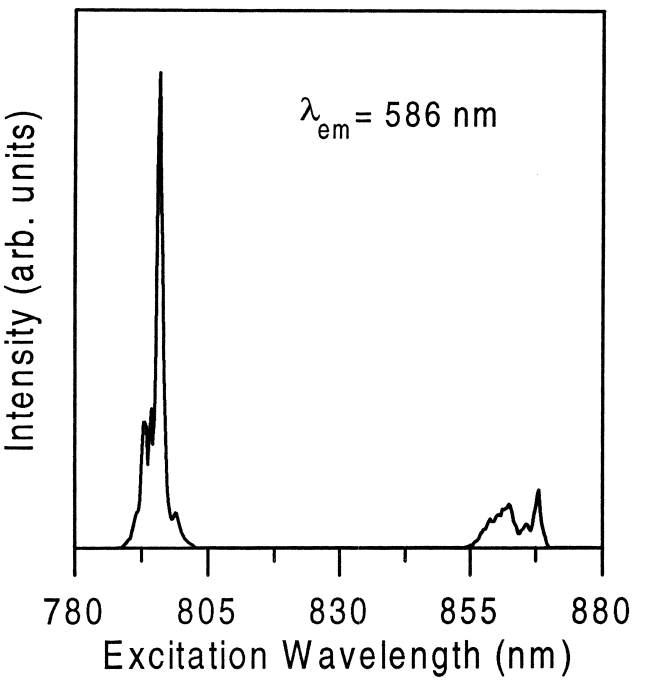

Fig. 6. Excitation spectrum of the 586 nm line, corrected for the spectral variation of the laser intensity. Measurements correspond to 77 K.

distance between excited centres [6]. As a consequence, there will be, in general, a noticeable similarity between the excitation spectrum corresponding to the upconverted emission and that obtained by the direct emission from the $^4F_{3/2}$ level. As mentioned above this is the case for the UV and VIS upconverted emissions.

On the other hand, in the limit of very small upconversion rates, the upconversion emission intensity (I_{em}) depends on the incident pump power (P_{pump}) according to the relation $I_{em} \propto (P_{pump})^n$, where n is the number of photons involved in the pumping mechanism, whereas in the case of very large upconversion rates $I_{em} \propto (P_{pump})^1$ for the upper states or even less than $(P_{pump})^1$ for intermediate states [7]. In our case, the dependence of the intensity of the three visible lines (526, 586 and 657 nm) on the pump power gives a value of 1.5 for n, which indicates a two photon upconversion process. On the other hand, the logarithmic plot of the blue lines (415 and 449 nm) and the UV line (382 nm) as a function of the laser power presents a slope of 2.2, which indicates that more than two IR photons are needed to reach the emission level. The values obtained suggest that, in this crystal, we are dealing with quite a strong ETU process for both UV and VIS upconverted emissions.

The temporal evolution of the upconverted emissions was obtained by exciting the samples in resonance with the $^4F_{3/2}$ level. All the experimental decays present a rapid initial decay followed by a longer nonexponential decay. As an example, the logarithmic plot of the experimental decay of the 586 nm emission at 77 K is shown in Fig. 7. Similar temporal evolutions are observed for the UV and blue emissions. The long term part of the decay curves of the upconverted VIS lines is much longer (≈110 μs) than that of the $^4G_{7/2}$ state under direct excitation (the lifetime values of the $^4G_{7/2}$ and $^4G_{5/2}$ levels obtained under direct excitation, which are too short to be measured with our equipment, have been measured to be less than 10 ns in fluoride crystals [8]). This behaviour suggests that we are dealing with a typical ETU process [8]. The decays of the upconverted blue and UV emissions also show a long term component of about 43 μs, but in this case if we assume, as indicated in Fig. 2, that these emissions come from level $^2P_{3/2}$, it is not possible to assign them unambiguously to an ETU process due to the metastable character of this level. Nevertheless, both the VIS and UV emissions show short risetimes (0.6 and 0.8 μs, respectively), which are also the fingerprints of ETU processes [9]. On the other hand, the short term component of the decay could be related to the existence of migration-assisted upconversion processes [8].

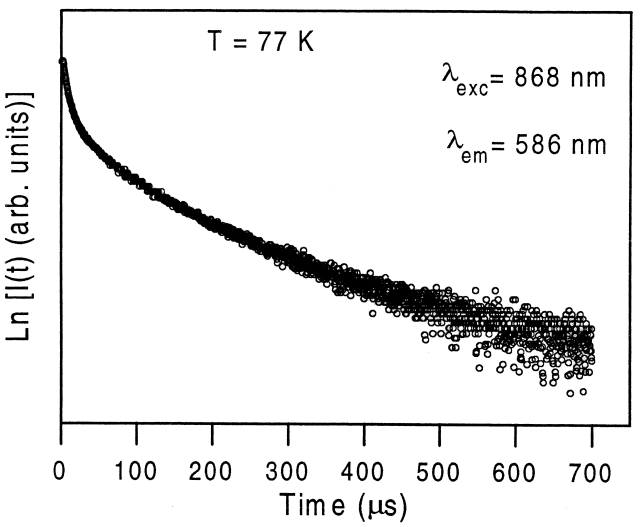

Fig. 7. Logarithmic plot of the experimental emission decay curve of the 586 nm emission obtained under excitation in resonance with the $^4F_{3/2}$ level. Data correspond to 77 K.

In order to identify each upconverted emission band, we used the low temperature emission spectrum given in Fig. 4a and the energy level diagram of Nd^{3+} in this crystal shown in Fig. 2. The three main VIS bands (526, 586 and 657 nm) observed in the emission spectrum have been reported in other Nd-doped materials, and attributed to transitions from the $^4G_{7/2}$ and $^4G_{5/2}$ levels [10–12]. As shown in Fig. 2 the analysis of the energy level diagram and the upconverted emission spectrum suggests that these bands can originate from the $^4G_{7/2}$ level. In addition, the decay curves are identical for these emissions, which shows they originate from the same level or group of levels. So the bands can be attributed to the following radiative transitions: $^4G_{7/2} \rightarrow {}^4I_{9/2}$ (526 nm), $^4G_{7/2} \rightarrow {}^4I_{11/2}$ (586 nm), and $^4G_{7/2} \rightarrow {}^4I_{13/2}$ (657 nm).

With respect to the blue and UV bands, the most probable origin of the upconverted fluorescence seems to be the $^2P_{3/2}$ level, although the level reached by upconversion could be $^4D_{3/2}$, $^4D_{5/2}$, $^4D_{1/2}$ or even higher levels. In this case, the participation of three neodymium ions is necessary in the ETU process. This kind of three body ETU process has been found in other fluoride materials [13].

It is worth mentioning that both ESA and ETU processes can coexist, and although in the present case an ETU process seems to be more likely for the observed visible and UV luminescence, other possible mechanisms such as ESA cannot be disregarded.

5. Conclusions

The spectroscopic features of the absorption and emission of Nd^{3+} in a fluoroaluminate $Pb_5Al_3F_{19}$ (PAF) crystal have been analysed taking into account the structure of the host matrix. Two main crystal field sites have been identified for the rare earth in this crystal which may correspond to the two different crystallographic sites of Pb^{2+}.

Infrared-to-visible and -ultraviolet upconversion, under continuous wave and pulsed laser excitation, have been

observed. Analysis of the steady-state excitation spectra and of the decays of the upconverted emissions shows that the most likely mechanism for the observed upconversion emissions is an energy-transfer upconversion (ETU) process.

Acknowledgements

This work was supported by the Basque Country University (G21/98), Basque Country Government, and Spanish Government CICYT Ref. MAT97-1009.

References

[1] A.A. Kaminskii, in: M.J. Weber (Ed.), Crystalline Lasers: Physical Processes and Operating Schemes, CRC Press, 1986.
[2] S.C. Abrahams, J. Ravez, Ferroelectrics 135 (1992) 21.
[3] S. Sarraute, Ph.D., Université de Bordeaux I, France, 1995.
[4] F. Auzel, C.R. Acad. Sci. (Paris) 262 (1996) 1016.
[5] F. Auzel, C.R. Acad. Sci. (Paris) 263 (1996) 819.
[6] J.H. Schloss, L.L. Chase, L.K. Smith, J. Lumin. 48/49 (1991) 857.
[7] M. Pollnau, D.R. Gamelin, S.R. Lüthi, H.U. Güdel, Phys. Rev. B 61 (2000) 3337.
[8] J.D. Zuegel, W. Seka, Appl. Opt. 38 (1999) 2714.
[9] M.P. Hehlen, G. Frei, H.U. Güdel, Phys. Rev. B 50 (1994) 16264.
[10] A.T. Stanley, E.A. Harris, T.M. Searle, J.M. Parker, J. Non-Cryst. Solids 161 (1993) 235.
[11] T. Tsuenoka, K. Kojima, S. Bojja, J. Non-Cryst. Solids 202 (1996) 297.
[12] R. Balda, J. Fernández, M. Sanz, A. de Pablos, J.M. Fdez-Navarro, J. Mugnier, Phys. Rev. B 61 (2000) 3384.
[13] L. de S. Menezes, Cid B. de Araujo, G.S. Maciel, Y. Messaddeq, M.A. Aegerter, Appl. Phys. Lett. 70 (1997) 683.